DESY 99-112
MPI/PhT/99-33
hep-ph/9908385
August 1999

ISSN 0418-9833

H^+H^- Pair Production at the Large Hadron Collider

A.A. Barrientos Bendezú
II. Institut für Theoretische Physik, Universität Hamburg,
Luruper Chaussee 149, 22761 Hamburg, Germany

B.A. Kniehl*
Max-Planck-Institut für Physik (Werner-Heisenberg-Institut),
Föhringer Ring 6, 80805 Munich, Germany

Abstract

We study the pair production of charged Higgs bosons at the CERN Large Hadron Collider in the context of the minimal supersymmetric extension of the standard model. We compare the contributions due to $q\bar{q}$ annihilation at the tree level and gg fusion, which proceeds at one loop. At small or large values of $\tan\beta$, H^+H^- production proceeds dominantly via $b\bar{b}$ annihilation, due to Feynman diagrams involving neutral CP-even Higgs bosons and top quarks, which come in addition to the usually considered Drell-Yan diagrams. In the case of gg fusion, the squark loop contributions may considerably enhance the well-known quark loop contributions.

PACS numbers: 12.60.Jv, 13.85.-t, 14.80.Cp

*Permanent address: II. Institut für Theoretische Physik, Universität Hamburg, Luruper Chaussee 149, 22761 Hamburg, Germany.

1 Introduction

One of the prime objectives of the CERN Large Hadron Collider (LHC) is the search for spin-zero particles which remain in the physical spectrum after the elementary-particle masses have been generated through the Higgs mechanism of electroweak symmetry breaking [1]. Should the world be supersymmetric, then the Higgs sector is more complicated than in the standard model (SM), which predicts just one scalar Higgs boson. The Higgs sector of the minimal supersymmetric extension of the SM (MSSM) consists of a two-Higgs-doublet model (2HDM) and accommodates five physical Higgs bosons: the neutral CP-even h^0 and H^0 bosons, the neutral CP-odd A^0 boson, and the charged $H^\pm$-boson pair. At the tree level, the MSSM Higgs sector has two free parameters, which are usually taken to be the mass m_{A^0} of the A^0 boson and the ratio $\tan\beta = v_2/v_1$ of the vacuum expectation values of the two Higgs doublets.

The discovery of the $H^\pm$ bosons would prove wrong the SM and, at the same time, give strong support to the MSSM. The logistics of the $H^\pm$-boson search at the LHC may be summarized as follows. For $H^\pm$-boson masses $m_H < m_t - m_b$, the dominant production mechanisms are $gg, q\bar{q} \to t\bar{t}$ followed by $t \to bH^+$ [1].[1] The dominant decay mode of $H^\pm$ bosons in this mass range is $H^+ \to \bar{\tau}\nu_\tau$ unless $\tan\beta < \sqrt{m_c/m_\tau} \approx 1$ [1]. In contrast to the SM top-quark events, this signature violates lepton universality, a criterion which is routinely applied in ongoing $H^\pm$-boson searches at the Fermilab $p\bar{p}$ collider Tevatron [2]. For larger values of m_H, the most copious sources of $H^\pm$ bosons are provided by $g\bar{b} \to \bar{t}H^+$ [3], $gg \to \bar{t}bH^+$ [4], and $qb \to q'bH^+$ [5]. The preferred decay channel is then $H^+ \to t\bar{b}$, independently of $\tan\beta$ [1]. An interesting alternative is to produce $H^\pm$ bosons in association with $W^\mp$ bosons, so that the leptonic decays of the latter may serve as a trigger for the $H^\pm$-boson search. The dominant subprocesses of $W^\pm H^\mp$ associated production are $b\bar{b} \to W^\pm H^\mp$ at the tree level and $gg \to W^\pm H^\mp$ at one loop, which were investigated for $m_b = 0$ and small values of $\tan\beta$ ($0.3 \leq \tan\beta \leq 2.3$) in Ref. [6] and recently, without these restrictions, in Ref. [7]. A careful signal-versus-background analysis, based on the analytic results of Ref. [7], was recently reported in Ref. [8].

In this paper, we investigate H^+H^- pair production in the MSSM. At the tree level, this proceeds via $q\bar{q}$ annihilation, $q\bar{q} \to H^+H^-$, where $q = u, d, s, c, b$. The Drell-Yan process, where a photon and a Z-boson are exchanged in the s channel (see upper Feynman diagram in Fig. 1) has been studied by a number of authors [9]. As pointed out in Ref. [7], in the case $q = b$, there are additional Feynman diagrams involving the h^0 and H^0 bosons in the s channel and the top quark in the t channel (see middle and lower diagrams in Fig. 1). As we shall see later on, for small or large values of $\tan\beta$, their contribution greatly exceeds the one due to the Drell-Yan process, which is independent of $\tan\beta$. To our knowledge, these additional diagrams have not been considered elsewhere in the literature. At one loop, H^+H^- pair production receives an additional contribution from gg fusion, $gg \to H^+H^-$. Although the cross section of gg fusion is suppressed by two powers of α_s relative to the one of $q\bar{q}$ annihilation, it is expected to yield a

[1] Here and in the following, the charge-conjugate processes will not be explicitly mentioned.

comparable contribution at multi-TeV hadron colliders, due to the overwhelming gluon luminosity. In the 2HDM, gg fusion is mediated by heavy-quark loops (see upper two rows in Fig. 2) [10,11]. We calculated these QCD contributions and found full agreement with the analytical and numerical results presented in Ref. [11]. In the MSSM, there are additional QCD contributions induced by squark loops (see lower three rows in Fig. 2), which we shall present here.

As for $b\bar{b}$ annihilation, it should be noted that the treatment of bottom as an active flavour inside the colliding hadrons leads to an effective description, which comprises contributions from the higher-order subprocesses $gb \to H^+H^-b$, $g\bar{b} \to H^+H^-\bar{b}$, and $gg \to H^+H^-b\bar{b}$. If all these subprocesses are to be explicitly included along with $b\bar{b} \to H^+H^-$, then it is necessary to employ a judiciously subtracted parton density function (PDF) for the bottom quark in order to avoid double counting [3,12]. The evaluation of $b\bar{b} \to H^+H^-$ with an unsubtracted bottom PDF is expected to slightly overestimate the true cross section [3,12]. For simplicity, we shall nevertheless adopt this effective approach in our analysis, keeping in mind that a QCD-correction factor below unity is to be applied.

The circumstance that the spectrum of states is more than doubled if one passes from the SM to the MSSM gives rise to a proliferation of parameters, which weakens the predictability of the theory. A canonical method to reduce the number of parameters is to embed the MSSM into a grand unified theory (GUT), e.g., a suitable supergravity (SUGRA) model, in such a way that it is recovered in the low-energy limit. The MSSM thus constrained is described by the following parameters at the GUT scale, which come in addition to $\tan\beta$ and m_A: the universal sfermion mass, m_0; the universal gaugino mass, $m_{1/2}$; the trilinear Higgs-sfermion coupling, A; the bilinear Higgs coupling, B; and the Higgs-higgsino mass parameter, μ. The number of parameters can be further reduced by making additional assumptions. Unification of the τ-lepton and b-quark Yukawa couplings at the GUT scale leads to a correlation between m_t and $\tan\beta$. Furthermore, if the electroweak symmetry is broken radiatively, then B and μ are determined up to the sign of μ. Finally, it turns out that the MSSM parameters are nearly independent of the value of A, as long as $|A| \lesssim 500$ GeV at the GUT scale. Further details on the SUGRA-inspired MSSM scenario may be found in Ref. [13] and the references cited therein.

This paper is organized as follows. In Section 2, we shall list analytic results for the tree-level cross section of $q\bar{q} \to H^+H^-$, including the Yukawa-enhanced contributions for $q = b$, and the squark loop contribution to the $gg \to H^+H^-$ amplitude in the MSSM. The relevant Higgs-squark coupling constants and the squark loop form factors are relegated to Appendices A and B, respectively. In Section 3, we shall present quantitative predictions for the inclusive cross section of $pp \to H^+H^- + X$ at the LHC adopting the SUGRA-inspired MSSM. Section 4 contains our conclusions.

2 Analytic results

We start by defining the kinematics of the inclusive reaction $AB \to H^+H^- + X$, where A and B are colliding hadrons, which are taken to be massless. Let $\sqrt{S}$ be the energy of

the initial state and y and p_T the rapidity and transverse momentum of the H^+ boson in the centre-of-mass (c.m.) system of the collision. By four-momentum conservation, $m_T \cosh y \leq \sqrt{S}/2$, where $m_T = \sqrt{m_H^2 + p_T^2}$ is the transverse mass of the $H^\pm$ bosons, with mass m_H. The hadron A is characterized by its PDF's $F_{a/A}(x_a, M_a)$, where x_a is the fraction of the four-momentum of A which is carried by the (massless) parton a ($p_a = x_a p_A$), M_a is the factorization scale, and similarly for B. The Mandelstam variables $s = (p_a + p_b)^2$, $t = (p_a - p_{H^+})^2$, and $u = (p_b - p_{H^+})^2$ at the parton level are thus related to S, y, and p_T by $s = x_a x_b S$, $t = m_H^2 - x_a\sqrt{S} m_T \exp(-y)$, and $u = m_H^2 - x_b\sqrt{S} m_T \exp(y)$, respectively. Notice that $sp_T^2 = tu - m_H^4$. In the parton model, the differential cross section of $AB \to H^+H^- + X$ is given by

$$\frac{d^2\sigma}{dy\, dp_T^2}(AB \to H^+H^- + X) = \sum_{a,b} \int_{\bar{x}_a}^1 dx_a\, F_{a/A}(x_a, M_a) F_{b/B}(x_b, M_b) \frac{x_b s}{m_H^2 - t} \times \frac{d\sigma}{dt}(ab \to H^+H^-), \tag{1}$$

where $\bar{x}_a = m_T \exp(y)/[\sqrt{S} - m_T \exp(-y)]$ and $x_b = x_a m_T \exp(-y)/[x_a\sqrt{S} - m_T \exp(y)]$. The parton-level cross section is calculated from the $ab \to H^+H^-$ transition-matrix element $\mathcal{T}$ as $d\sigma/dt = \overline{|\mathcal{T}|^2}/(16\pi s^2)$, where the average is over the spin and colour degrees of freedom of the partons a and b.

We now turn to the specific subprocesses $ab \to H^+H^-$. We work in the MSSM, adopting the Feynman rules from Ref. [14]. For convenience, we introduce the short-hand notations $s_w = \sin\theta_w$, $c_w = \cos\theta_w$, $s_\alpha = \sin\alpha$, $c_\alpha = \cos\alpha$, $s_\beta = \sin\beta$, $c_\beta = \cos\beta$, $s_{2\beta} = \sin(2\beta)$, $c_{2\beta} = \cos(2\beta)$, $s_\pm = \sin(\alpha \pm \beta)$, and $c_\pm = \cos(\alpha \pm \beta)$, where θ_w is the electroweak mixing angle, α is the mixing angle that rotates the weak CP-even Higgs eigenstates into the mass eigenstates h^0 and H^0, and $\tan\beta = v_2/v_1$ is the ratio of the vacuum expectation values of the two Higgs doublets. We neglect the Yukawa couplings of the first- and second-generation quarks. We treat the b and $\bar{b}$ quarks as active partons inside the colliding hadrons A and B. This should be a useful picture at the energies of interest here, $\sqrt{S} > 2m_H$. For consistency with the underlying infinite-momentum frame, we neglect the bottom-quark mass, m_b. However, we must not suppress terms proportional to m_b in the Yukawa couplings, since they generally dominate the related m_t-dependent terms if $\tan\beta$ is large enough, typically for $\tan\beta \gtrsim \sqrt{m_t/m_b} \approx 6$. This is obvious for the $H^-\bar{b}t$ vertex, which has the Feynman rule [14]

$$i2^{-1/4} G_F^{1/2} [m_t \cot\beta (1 + \gamma_5) + m_b \tan\beta (1 - \gamma_5)], \tag{2}$$

where G_F is Fermi's constant and we have neglected the Cabibbo-Kobayashi-Maskawa mixing, i.e., $V_{tb} = 1$.

The tree-level diagrams for $b\bar{b} \to H^+H^-$ in the MSSM are depicted in Fig. 1. The resulting parton-level cross section reads

$$\frac{d\sigma}{dt}(b\bar{b} \to H^+H^-) = \frac{G_F^2}{3\pi s} \left[|S|^2 + 4p_T^2 \left(|V + T_+|^2 + |A + T_-|^2 \right) \right], \tag{3}$$

where

$$
\begin{aligned}
S &= g_{H^+H^-h^0} g_{h^0bb} \mathcal{P}_{h^0}(s) + g_{H^+H^-H^0} g_{H^0bb} \mathcal{P}_{H^0}(s) - \frac{m_b m_t^2}{2m_W^2\,(m_t^2 - t)}, \\
V &= g_{H^+H^-Z} v_{Zbb} \mathcal{P}_Z(s) + g_{H^+H^-\gamma} v_{\gamma bb} \mathcal{P}_\gamma(s), \\
A &= g_{H^+H^-Z} a_{Zbb} \mathcal{P}_Z(s), \\
T_\pm &= \frac{m_t^2 \cot^2\beta \pm m_b^2 \tan^2\beta}{8m_w^2\,(m_t^2 - t)},
\end{aligned}
\tag{4}
$$

with couplings

$$
\begin{aligned}
g_{H^+H^-h^0} &= m_W s_- - \frac{m_Z s_+ c_{2\beta}}{2c_w}, \qquad g_{h^0bb} = \frac{m_b s_\alpha}{2m_W c_\beta}, \\
g_{H^+H^-H^0} &= -m_W c_- + \frac{m_Z c_+ c_{2\beta}}{2c_w}, \qquad g_{H^0bb} = -\frac{m_b c_\alpha}{2m_W c_\beta}, \\
g_{H^+H^-Z} &= -\frac{c_w^2 - s_w^2}{2c_w}, \qquad v_{Zbb} = -\frac{I_b - 2s_w^2 Q_b}{2c_w}, \qquad a_{Zbb} = -\frac{I_b}{2c_w}, \\
g_{H^+H^-\gamma} &= -s_w, \qquad v_{\gamma bb} = -s_w Q_b,
\end{aligned}
\tag{5}
$$

weak isospin $I_b = -1/2$, and electric charge $Q_b = -1/3$. Here,

$$
\mathcal{P}_X(s) = \frac{1}{s - m_X^2 + i m_X \Gamma_X}
\tag{6}
$$

is the propagator function of particle X, with mass m_X and total decay width Γ_X. We recover the well-known Drell-Yan cross section of $q\bar{q} \to H^+H^-$ [9] from Eq. (3) by putting $S = T_\pm = 0$ and substituting $b \to q$. The approximation $S = T_\pm = 0$ is justified for the quarks of the first and second generations, $q = u, d, s, c$, because S and $T_\pm$ are then suppressed by the smallness of the corresponding Yukawa couplings. However, the S and $T_\pm$ terms give rise to sizeable contributions in the case of $q = b$, especially at small or large values of $\tan\beta$. The full cross section of $q\bar{q}$ annihilation is obtained by complementing the $b\bar{b}$-initiated cross section of Eq. (3) with the Drell-Yan cross sections for $q = u, d, s, c$.

The one-loop diagrams for $gg \to H^+H^-$ in the MSSM are displayed in Fig. 2. As for the quark loops, our analytical results fully agree with those listed in Ref. [11], and there is no need to repeat them here. In the squark case, the $\mathcal{T}$-matrix elements corresponding to the triangle and box diagrams are found to be

$$
\begin{aligned}
\tilde{\mathcal{T}}_\triangle &= \frac{G_F m_W^2}{\sqrt{2}} \frac{\alpha_s(\mu_r)}{\pi} \varepsilon_\mu^c(p_a) \varepsilon_\nu^c(p_b) A_1^{\mu\nu} \tilde{F}_\triangle, \\
\tilde{\mathcal{T}}_\square &= \frac{G_F m_W^2}{\sqrt{2}} \frac{\alpha_s(\mu_r)}{\pi} \varepsilon_\mu^c(p_a) \varepsilon_\nu^c(p_b) \left(A_1^{\mu\nu} \tilde{F}_\square + A_2^{\mu\nu} \tilde{G}_\square \right),
\end{aligned}
\tag{7}
$$

respectively, where $\alpha_s(\mu_r)$ is the strong coupling constant at renormalization scale μ_r, $\varepsilon_\mu^c(p_a)$ is the polarization four-vector of gluon a and similarly for gluon b, it is summed

over the colour index $c = 1, \ldots, 8$,

$$A_1^{\mu\nu} = g^{\mu\nu} - \frac{2}{s} p_a^\nu p_b^\mu,$$
$$A_2^{\mu\nu} = g^{\mu\nu} + \frac{2}{p_T^2}\left(\frac{m_H^2}{s} p_a^\nu p_b^\mu + \frac{u - m_H^2}{s} p_a^\nu p_{H^+}^\mu + \frac{t - m_H^2}{s} p_b^\mu p_{H^+}^\nu + p_{H^+}^\mu p_{H^+}^\nu\right), \qquad (8)$$

and the form factors $\tilde{F}_\triangle$, $\tilde{F}_\square$, and $\tilde{G}_\square$ are listed in Appendix B. Due to Bose symmetry, $\tilde{\mathcal{T}}_\triangle$ and $\tilde{\mathcal{T}}_\square$ are invariant under the simultaneous replacements $\mu \leftrightarrow \nu$ and $p_a \leftrightarrow p_b$. Consequently, $\tilde{F}_\triangle$, $\tilde{F}_\square$, and $\tilde{G}_\square$ are symmetric in t and u.

The parton-level cross section of $b\bar{b} \to H^+H^-$ including both quark and squark contributions is then given by

$$\frac{d\sigma}{dt}(gg \to H^+H^-) = \frac{G_F^2 \alpha_s^2(\mu_r)}{256(2\pi)^3}\left[\left|\sum_{Q=t,b} C_\triangle^Q F_\triangle^Q + F_\square - \frac{2m_W^2}{s}\left(\tilde{F}_\triangle + \tilde{F}_\square\right)\right|^2 + \left|G_\square - \frac{2m_W^2}{s}\tilde{G}_\square\right|^2 + |H_\square|^2\right], \qquad (9)$$

where the generalized coupling $C_\triangle^Q$ and the form factors $F_\triangle^Q$, $F_\square$, $G_\square$, and $H_\square$ may be found in Eq. (8) and Appendix A of Ref. [11], respectively.

3 Phenomenological implications

We are now in a position to explore the phenomenological implications of our results. The SM input parameters for our numerical analysis are taken to be $G_F = 1.16639 \cdot 10^{-5}$ GeV^{-2} [15], $m_W = 80.394$ GeV, $m_Z = 91.1867$ GeV, $m_t = 174.3$ GeV [16], and $m_b = 4.7$ GeV. We adopt the lowest-order set CTEQ5L [17] of proton PDF's. We evaluate $\alpha_s(\mu_r)$ from the lowest-order formula [15] with $n_f = 5$ quark flavours and asymptotic scale parameter $\Lambda_{\rm QCD}^{(5)} = 146$ MeV [17]. We identify the renormalization and factorization scales with the H^+H^- invariant mass, $\mu_r^2 = M_a^2 = M_b^2 = s$. For our purposes, it is useful to replace m_A by m_H, the mass of the $H^\pm$ bosons to be produced, in the set of MSSM input parameters. We vary $\tan\beta$ and m_H in the ranges $1 < \tan\beta < 40 \approx m_t/m_b$ and 120 GeV $< m_H <$ 550 GeV, respectively. As for the GUT parameters, we choose $m_{1/2} = 100$ GeV, $A = 0$, and $\mu < 0$, and tune m_0 so as to be consistent with the desired value of m_H. All other MSSM parameters are then determined according to the SUGRA-inspired scenario as implemented in the program package SUSPECT [18]. We do not impose the unification of the τ-lepton and b-quark Yukawa couplings at the GUT scale, which would just constrain the allowed $\tan\beta$ range without any visible effect on the results for these values of $\tan\beta$.

We now study the total cross section of $pp \to H^+H^- + X$ at the LHC, with c.m. energy $\sqrt{S} = 14$ TeV. In Fig. 3, the full contributions due to $q\bar{q}$ annihilation (dashed line) and gg fusion (solid line) are displayed as functions of $\tan\beta$ for $m_H = 200$ GeV. For

comparison, also the Drell-Yan contributions to $q\bar{q}$ annihilation for $q = u, d, s, c, b$ (dotted line) and the quark loop contribution to gg fusion (dot-dashed line), which is the full one-loop result for gg-fusion in the 2HDM, are shown. In the case of $q\bar{q}$ annihilation, as anticipated in Section 1, the Yukawa-enhanced contribution for $q = b$ greatly enhances the conventional Drell-Yan cross section for large values of $\tan\beta$, by more than a factor of three for $\tan\beta = 40$. The expected enhancement for small $\tan\beta$ is invisible, since solutions with $\tan\beta \lesssim 2$ are excluded in the SUGRA-inspired MSSM for our choice of input parameters. As for gg fusion, the dot-dashed line nicely agrees with Fig. 6 of Ref. [11]. The quark loop contribution exhibits a minimum at $\tan\beta \approx \sqrt{m_t/m_b} \approx 6$. This may be understood by observing that the average strength of the $H^-\bar{b}t$ coupling in Eq. (2), proportional to $\sqrt{m_t^2 \cot^2\beta + m_b^2 \tan^2\beta}$, is then minimal [11]. Passing from the 2HDM to the MSSM, we need to coherently add the squark loop contribution according to Eq. (9). We observe that this leads to a significant rise in cross section, by up to 50%, unless $\tan\beta$ is close to 10. Nevertheless, the full tree-level cross section is dominant for all values of $\tan\beta$.

In Fig. 4, the m_H dependence of the full $q\bar{q}$-annihilation (dashed lines) and gg-fusion cross sections (solid lines) is studied for $\tan\beta = 1.5$, 6, and 30. As we have already seen in Fig. 3, $q\bar{q}$ annihilation always dominates. Its contribution modestly exceeds the one due to gg fusion, by a factor of three or less, if $\tan\beta \approx 1.5$ or 30 and $m_H \gtrsim 200$ GeV, but it is more than one order of magnitude larger if $m_H \lesssim m_t$. The gg-fusion contribution is greatly suppressed if $\tan\beta \approx 6$, independently of m_H. For all values of $\tan\beta$, the latter exhibits a dip located about $m_H = m_t$, which arises from resonating top-quark propagators in the quark box form factors. (In the case of $\tan\beta = 1.5$, this dip lies in the excluded m_H range.) This feature may also be seen in Fig. 5 of Ref. [11], where the quark loop contribution is shown separately. We note in passing that we also find good agreement with that figure.

For a comparison with future experimental data, the $q\bar{q}$-annihilation and gg-fusion channels should be combined. From Fig. 4, we read off that the total cross section of $pp \to H^+H^- + X$ at the LHC is predicted to be 200 fb (1 fb) in the considered MSSM scenario if $\tan\beta = 30$ and $m_H = 120$ GeV (500 GeV). If we assume the integrated luminosity per year to be at its design value of $L = 100$ fb^{-1} for each of the two LHC experiments, ATLAS and CMS, then this translates into about 40.000 (200) signal events per year.

4 Conclusions

We studied the hadroproduction of H^+H^- pairs within the MSSM, adopting a SUGRA-inspired scenario. We included the contributions from $q\bar{q}$ annihilation and gg fusion to lowest order and provided full analytic results. Our analysis reaches beyond previous studies [9,10,11] in two important respects. In the case of $q\bar{q}$ annihilation, we demonstrated that previously neglected Yukawa-type contributions in the $b\bar{b}$ channel lead to a substantial increase in cross section if $\tan\beta$ is large, by more than a factor of three for $\tan\beta = 40$.

In the case of gg fusion, we upgraded a previous result [11], which we confirmed, from the 2HDM to the MSSM by including the contributions induced by virtual squarks. As a result, the gg-fusion cross section may be significantly enhanced, by up to 50%, depending on $\tan\beta$. Should the MSSM be realized in nature, then H^+H^- pair production will provide a copious source of charged Higgs bosons at the LHC, with an annual yield of up to 40.000 signal events, which amounts to 80.000 charged Higgs bosons per year.

Acknowledgements

B.A.K. thanks the Theory Group of the Werner-Heisenberg-Institut for the hospitality extended to him during a visit when this paper was finalized. The work of A.A.B.B. was supported by the Friedrich-Ebert-Stiftung through Grant No. 219747.

A Higgs-squark couplings

In this appendix, we collect the couplings of the h^0, H^0, and $H^\pm$ bosons to the squarks $\tilde{q}_i$, with $q = t, b$ and $i = 1, 2$, which are relevant for our analysis. Defining the mixing matrix which rotates the left- and right-handed squark fields, $\tilde{q}_L$ and $\tilde{q}_R$, into the mass eigenstates $\tilde{q}_i$ as

$$\mathcal{M}^{\tilde{q}} = \begin{pmatrix} \cos\theta_{\tilde{q}} & \sin\theta_{\tilde{q}} \\ -\sin\theta_{\tilde{q}} & \cos\theta_{\tilde{q}} \end{pmatrix}, \tag{A.1}$$

we have [14]

$$\begin{pmatrix} g_{h^0\tilde{t}_1\tilde{t}_1} & g_{h^0\tilde{t}_1\tilde{t}_2} \\ g_{h^0\tilde{t}_2\tilde{t}_1} & g_{h^0\tilde{t}_2\tilde{t}_2} \end{pmatrix} = \mathcal{M}^{\tilde{t}} \begin{pmatrix} \frac{m_Z s_+ (I_t^3 - s_w^2 Q_t)}{c_w} - \frac{m_t^2 c_\alpha}{m_W s_\beta} & -\frac{m_t(\mu s_\alpha + A_t c_\alpha)}{2 m_W s_\beta} \\ -\frac{m_t(\mu s_\alpha + A_t c_\alpha)}{2 m_W s_\beta} & \frac{m_Z s_+ s_w^2 Q_t}{c_w} - \frac{m_t^2 c_\alpha}{m_W s_\beta} \end{pmatrix} \left(\mathcal{M}^{\tilde{t}}\right)^T,$$

$$\begin{pmatrix} g_{h^0\tilde{b}_1\tilde{b}_1} & g_{h^0\tilde{b}_1\tilde{b}_2} \\ g_{h^0\tilde{b}_2\tilde{b}_1} & g_{h^0\tilde{b}_2\tilde{b}_2} \end{pmatrix} = \mathcal{M}^{\tilde{b}} \begin{pmatrix} \frac{m_Z s_+ (I_b^3 - s_w^2 Q_b)}{c_w} + \frac{m_b^2 s_\alpha}{m_W c_\beta} & \frac{m_b(\mu c_\alpha + A_b s_\alpha)}{2 m_W c_\beta} \\ \frac{m_b(\mu c_\alpha + A_b s_\alpha)}{2 m_W c_\beta} & \frac{m_Z s_+ s_w^2 Q_b}{c_w} + \frac{m_b^2 s_\alpha}{m_W c_\beta} \end{pmatrix} \left(\mathcal{M}^{\tilde{b}}\right)^T,$$

$$\begin{pmatrix} g_{H^0\tilde{t}_1\tilde{t}_1} & g_{H^0\tilde{t}_1\tilde{t}_2} \\ g_{H^0\tilde{t}_2\tilde{t}_1} & g_{H^0\tilde{t}_2\tilde{t}_2} \end{pmatrix} = \mathcal{M}^{\tilde{t}} \begin{pmatrix} -\frac{m_Z c_+ (I_t^3 - s_w^2 Q_t)}{c_W} - \frac{m_t^2 s_\alpha}{m_W s_\beta} & \frac{m_t(\mu c_\alpha - A_t s_\alpha)}{2 m_W s_\beta} \\ \frac{m_t(\mu c_\alpha - A_t s_\alpha)}{2 m_W s_\beta} & -\frac{m_Z c_+ s_w^2 Q_t}{c_w} - \frac{m_t^2 s_\alpha}{m_W s_\beta} \end{pmatrix} \left(\mathcal{M}^{\tilde{t}}\right)^T,$$

$$\begin{pmatrix} g_{H^0\tilde{b}_1\tilde{b}_1} & g_{H^0\tilde{b}_1\tilde{b}_2} \\ g_{H^0\tilde{b}_2\tilde{b}_1} & g_{H^0\tilde{b}_2\tilde{b}_2} \end{pmatrix} = \mathcal{M}^{\tilde{b}} \begin{pmatrix} -\frac{m_Z c_+ (I_b^3 - s_w^2 Q_b)}{c_w} - \frac{m_b^2 c_\alpha}{m_W c_\beta} & \frac{m_b(\mu s_\alpha - A_b c_\alpha)}{2 m_W c_\beta} \\ \frac{m_b(\mu s_\alpha - A_b c_\alpha)}{2 m_W c_\beta} & -\frac{m_Z c_+ s_w^2 Q_b}{c_w} - \frac{m_b^2 c_\alpha}{m_W c_\beta} \end{pmatrix} \left(\mathcal{M}^{\tilde{b}}\right)^T,$$

$$\begin{pmatrix} g_{H^+\tilde{t}_1\tilde{b}_1} & g_{H^+\tilde{t}_1\tilde{b}_2} \\ g_{H^+\tilde{t}_2\tilde{b}_1} & g_{H^+\tilde{t}_2\tilde{b}_2} \end{pmatrix} = \mathcal{M}^{\tilde{t}} \begin{pmatrix} \frac{-m_W^2 s_{2\beta} + m_t^2 \cot\beta + m_b^2 \tan\beta}{\sqrt{2} m_W} & \frac{m_b(\mu + A_b \tan\beta)}{\sqrt{2} m_W} \\ \frac{m_t(\mu + A_t \cot\beta)}{\sqrt{2} m_W} & \frac{m_t m_b(\tan\beta + \cot\beta)}{\sqrt{2} m_W} \end{pmatrix} \left(\mathcal{M}^{\tilde{b}}\right)^T,$$

$$\begin{pmatrix} g_{H^+H^-\tilde{t}_1\tilde{t}_1} & g_{H^+H^-\tilde{t}_1\tilde{t}_2} \\ g_{H^+H^-\tilde{t}_2\tilde{t}_1} & g_{H^+H^-\tilde{t}_2\tilde{t}_2} \end{pmatrix} = \mathcal{M}^{\tilde{t}} \begin{pmatrix} \frac{c_{2\beta}[I_t^3(1-2c_w^2) - s_w^2 Q_t]}{2 c_w^2} - \frac{m_b^2 \tan^2\beta}{2 m_W^2} & 0 \\ 0 & \frac{c_{2\beta} s_w^2 Q_t}{2 c_w^2} - \frac{m_t^2 \cot^2\beta}{2 m_W^2} \end{pmatrix} \left(\mathcal{M}^{\tilde{t}}\right)^T,$$

$$\begin{pmatrix} g_{H^+H^-\tilde{b}_1\tilde{b}_1} & g_{H^+H^-\tilde{b}_1\tilde{b}_2} \\ g_{H^+H^-\tilde{b}_2\tilde{b}_1} & g_{H^+H^-\tilde{b}_2\tilde{b}_2} \end{pmatrix} = \mathcal{M}^{\tilde{b}} \begin{pmatrix} \frac{c_{2\beta}[I_b^3(1-2c_w^2)-s_w^2 Q_b]}{2c_w^2} - \frac{m_t^2 \cot^2\beta}{2m_W^2} & 0 \\ 0 & \frac{c_{2\beta}s_w^2 Q_b}{2c_w^2} - \frac{m_b^2 \tan^2\beta}{2m_W^2} \end{pmatrix} \left(\mathcal{M}^{\tilde{b}}\right)^T . \tag{A.2}$$

The corresponding Feynman rules emerge by multiplying these couplings with ig, where g is the SU(2) coupling constant. Similar relations apply for the squarks of the first and second generations, which are also included in our analysis. However, in these cases, we neglect terms which are suppressed by the smallness of the corresponding light-quark masses.

B Squark loop form factors

In this appendix, we express the squark triangle and box form factors, $\tilde{F}_\triangle$, $\tilde{F}_\square$, and $\tilde{G}_\square$, in terms of the standard scalar three- and four-point functions,

$$\begin{aligned} &C_0\left(p_1^2,(p_2-p_1)^2,p_2^2,m_0^2,m_1^2,m_2^2\right) \\ &= \int \frac{d^4q}{i\pi^2} \frac{1}{(q^2-m_0^2+i\epsilon)\left[(q+p_1)^2-m_1^2+i\epsilon\right]\left[(q+p_2)^2-m_2^2+i\epsilon\right]}, \\ &D_0\left(p_1^2,(p_2-p_1)^2,(p_3-p_2)^2,p_3^2,p_2^2,(p_3-p_1)^2,m_0^2,m_1^2,m_2^2,m_3^2\right) \\ &= \int \frac{d^4q}{i\pi^2} \frac{1}{(q^2-m_0^2+i\epsilon)\left[(q+p_1)^2-m_1^2+i\epsilon\right]\left[(q+p_2)^2-m_2^2+i\epsilon\right]\left[(q+p_3)^2-m_3^2+i\epsilon\right]}, \end{aligned} \tag{B.1}$$

which we evaluate numerically with the aid of the program package FF [19]. We have

$$\begin{aligned} \tilde{F}_\triangle = {} & g_{H^+H^-h^0}\mathcal{P}_{h^0}(s)\left[g_{h^0\tilde{t}_1\tilde{t}_1}F_1\left(s,m_{\tilde{t}_1}\right)+g_{h^0\tilde{t}_2\tilde{t}_2}F_1\left(s,m_{\tilde{t}_2}\right)\right. \\ & \left.+\, g_{h^0\tilde{b}_1\tilde{b}_1}F_1\left(s,m_{\tilde{b}_1}\right)+g_{h^0\tilde{b}_2\tilde{b}_2}F_1\left(s,m_{\tilde{b}_2}\right)\right] \\ & + g_{H^+H^-H^0}\mathcal{P}_{H^0}(s)\left[g_{H^0\tilde{t}_1\tilde{t}_1}F_1\left(s,m_{\tilde{t}_1}\right)+g_{H^0\tilde{t}_2\tilde{t}_2}F_1\left(s,m_{\tilde{t}_2}\right)\right. \\ & \left.+\, g_{H^0\tilde{b}_1\tilde{b}_1}F_1\left(s,m_{\tilde{b}_1}\right)+g_{H^0\tilde{b}_2\tilde{b}_2}F_1\left(s,m_{\tilde{b}_2}\right)\right] \\ & - g_{H^+H^-\tilde{t}_1\tilde{t}_1}F_1\left(s,m_{\tilde{t}_1}\right)-g_{H^+H^-\tilde{t}_2\tilde{t}_2}F_1\left(s,m_{\tilde{t}_2}\right) \\ & - g_{H^+H^-\tilde{b}_1\tilde{b}_1}F_1\left(s,m_{\tilde{b}_1}\right)-g_{H^+H^-\tilde{b}_2\tilde{b}_2}F_1\left(s,m_{\tilde{b}_2}\right), \\ \tilde{F}_\square = {} & g^2_{H^+\tilde{t}_1\tilde{b}_1}\left[F_2\left(h,s,t,u,m_{\tilde{t}_1},m_{\tilde{b}_1}\right)+\left(m_{\tilde{t}_1}\leftrightarrow m_{\tilde{b}_1}\right)\right] \\ & + g^2_{H^+\tilde{t}_1\tilde{b}_2}\left[F_2\left(h,s,t,u,m_{\tilde{t}_1},m_{\tilde{b}_2}\right)+\left(m_{\tilde{t}_1}\leftrightarrow m_{\tilde{b}_2}\right)\right] \\ & + g^2_{H^+\tilde{t}_2\tilde{b}_1}\left[F_2\left(h,s,t,u,m_{\tilde{t}_2},m_{\tilde{b}_1}\right)+\left(m_{\tilde{t}_2}\leftrightarrow m_{\tilde{b}_1}\right)\right] \\ & + g^2_{H^+\tilde{t}_2\tilde{b}_2}\left[F_2\left(h,s,t,u,m_{\tilde{t}_2},m_{\tilde{b}_2}\right)+\left(m_{\tilde{t}_2}\leftrightarrow m_{\tilde{b}_2}\right)\right], \end{aligned} \tag{B.2}$$

where $h = m_H^2$. $\tilde{G}_\Box$ is obtained from $\tilde{F}_\Box$ by substituting $F_2 \to F_3$. Here, we have introduced the auxiliary functions

$$
\begin{aligned}
F_1(s, m_{\tilde{q}}) &= 2 + 4m_{\tilde{q}}^2 C_0\left(0, 0, s, m_{\tilde{q}}^2, m_{\tilde{q}}^2, m_{\tilde{q}}^2\right), \\
F_2(h, s, t, u, m_{\tilde{t}}, m_{\tilde{b}}) &= -\frac{2}{s}\left(t_1 C_0^3 + u_1 C_0^5\right) + p_T^2 D_0^1 + 2m_{\tilde{t}}^2\left(D_0^1 + D_0^3 + D_0^5\right), \\
F_3(h, s, t, u, m_{\tilde{t}}, m_{\tilde{b}}) &= \frac{1}{s p_T^2}\Big\{s\left[-(t+u)C_0^2 + t^2 D_0^3 + u^2 D_0^5\right] - 2tt_1 C_0^4 - 2uu_1 C_0^6 \\
&\quad + (t^2 + u^2 - 2h^2) C_0^7 \\
&\quad + 2m_{\tilde{t}}^2\left[s\left(C_0^1 - C_0^2 + p_T^2 D_0^1 - tD_0^2 - uD_0^4\right) - t_1^2 D_0^3 - u_1^2 D_0^5\right] \\
&\quad + s m_{\tilde{t}}^2\left(m_{\tilde{t}}^2 - m_{\tilde{b}}^2\right)\left(2D_0^1 + D_0^2 + D_0^3 + D_0^4 + D_0^5\right)\Big\}, \qquad \text{(B.3)}
\end{aligned}
$$

where $t_1 = t - h$, $u_1 = u - h$, and

$$
\begin{aligned}
C_0^1 &= C_0\left(0, 0, s, m_{\tilde{b}}^2, m_{\tilde{b}}^2, m_{\tilde{b}}^2\right), \\
C_0^2 &= C_0\left(0, 0, s, m_{\tilde{t}}^2, m_{\tilde{t}}^2, m_{\tilde{t}}^2\right), \\
C_0^3 &= C_0\left(h, 0, t, m_{\tilde{b}}^2, m_{\tilde{t}}^2, m_{\tilde{t}}^2\right), \\
C_0^4 &= C_0\left(h, 0, t, m_{\tilde{t}}^2, m_{\tilde{b}}^2, m_{\tilde{b}}^2\right), \\
C_0^5 &= C_0\left(h, 0, u, m_{\tilde{b}}^2, m_{\tilde{t}}^2, m_{\tilde{t}}^2\right), \\
C_0^6 &= C_0\left(h, 0, u, m_{\tilde{t}}^2, m_{\tilde{b}}^2, m_{\tilde{b}}^2\right), \\
C_0^7 &= C_0\left(h, h, s, m_{\tilde{t}}^2, m_{\tilde{b}}^2, m_{\tilde{t}}^2\right), \\
D_0^1 &= D_0\left(h, 0, h, 0, t, u, m_{\tilde{b}}^2, m_{\tilde{t}}^2, m_{\tilde{t}}^2, m_{\tilde{b}}^2\right), \\
D_0^2 &= D_0\left(h, h, 0, 0, s, t, m_{\tilde{b}}^2, m_{\tilde{t}}^2, m_{\tilde{b}}^2, m_{\tilde{b}}^2\right), \\
D_0^3 &= D_0\left(h, h, 0, 0, s, t, m_{\tilde{t}}^2, m_{\tilde{b}}^2, m_{\tilde{t}}^2, m_{\tilde{t}}^2\right), \\
D_0^4 &= D_0\left(h, h, 0, 0, s, u, m_{\tilde{b}}^2, m_{\tilde{t}}^2, m_{\tilde{b}}^2, m_{\tilde{b}}^2\right), \\
D_0^5 &= D_0\left(h, h, 0, 0, s, u, m_{\tilde{t}}^2, m_{\tilde{b}}^2, m_{\tilde{t}}^2, m_{\tilde{t}}^2\right). \qquad \text{(B.4)}
\end{aligned}
$$

References

[1] Z. Kunszt and F. Zwirner, Nucl. Phys. B 385 (1992) 3, and references cited therein.

[2] F. Abe et al. (CDF Collaboration), Phys. Rev. D 54 (1996) 735;
B. Bevensee (for the CDF and D0 Collaborations), Report No. FERMILAB–Conf–98/155–E (May 1998), to be published in the proceedings of 33rd Rencontres de Moriond: QCD and High Energy Hadronic Interactions, Les Arcs, France, 21–28 March 1998.

[3] J.F. Gunion, H.E. Haber, F.E. Paige, W.-K. Tung and S.S.D. Willenbrock, Nucl. Phys. B 294 (1987) 621;
R.M. Barnett, H.E. Haber and D.E. Soper, Nucl. Phys. B 306 (1988) 697;
F.I. Olness and W.-K. Tung, Nucl. Phys. B 308 (1988) 813;
V. Barger, R.J.N. Phillips and D.P. Roy, Phys. Lett. B 324 (1994) 236.

[4] J.L. Diaz-Cruz and O.A. Sampayo, Phys. Rev. D 50 (1994) 6820.

[5] S. Moretti and K. Odagiri, Phys. Rev. D 55 (1997) 5627.

[6] D.A. Dicus, J.L. Hewett, C. Kao and T.G. Rizzo, Phys. Rev. D 40 (1989) 787.

[7] A.A. Barrientos Bendezú and B.A. Kniehl, Phys. Rev. D 59 (1998) 015009.

[8] S. Moretti and K. Odagiri, Phys. Rev. D 59 (1999) 055008.

[9] E. Eichten, I. Hinchliffe, K. Lane and C. Quigg, Rev. Mod. Phys. 56 (1984) 579; 58 (1986) 1065 (E);
N.G. Deshpande, X. Tata and D.A. Dicus, Phys. Rev. D 29 (1984) 1527.

[10] S.S.D. Willenbrock, Phys. Rev. D 35 (1987) 173;
J. Yi, M. Wen-Gan, H. Liang, H. Meng and Y. Zeng-Hui, J. Phys. G 24 (1998) 83.

[11] A. Krause, T. Plehn, M. Spira and P.M. Zerwas, Nucl. Phys. B 519 (1998) 85.

[12] D.A. Dicus and S. Willenbrock, Phys. Rev. D 39 (1989) 751;
D.A. Dicus and C. Kao, Phys. Rev. D 41 (1990) 832.

[13] A. Djouadi, J. Kalinowski, P. Ohmann and P.M. Zerwas, Z. Phys. C 74 (1997) 93.

[14] J.F. Gunion and H.E. Haber, Nucl. Phys. B 272 (1986) 1; B 402 (1993) 567 (E); B 278 (1986) 449;
J.F. Gunion, H.E. Haber, G. Kane and S. Dawson, The Higgs Hunter's Guide (Addison-Wesley, Redwood City, 1990).

[15] C. Caso et al. (Particle Data Group), Eur. Phys. J. C 3 (1998) 1.

[16] D. Abbaneo et al. (The LEP Collaborations ALEPH, DELPHI, L3, OPAL, the LEP Electroweak Working Group and the SLD Heavy Flavour and Electroweak Groups), Report No. CERN-EP/99-15 (February 1999).

[17] H.L. Lai et al. (CTEQ Collaboration), Report No. MSU-HEP-903100 and hep-ph/9903282 (March 1999).

[18] A. Djouadi, J.-L. Kneur and G. Moultaka, Report No. PM/98-27 and GDR-S-017 (1998).

[19] G.J. van Oldenborgh, Comput. Phys. Commun. 66 (1991) 1.

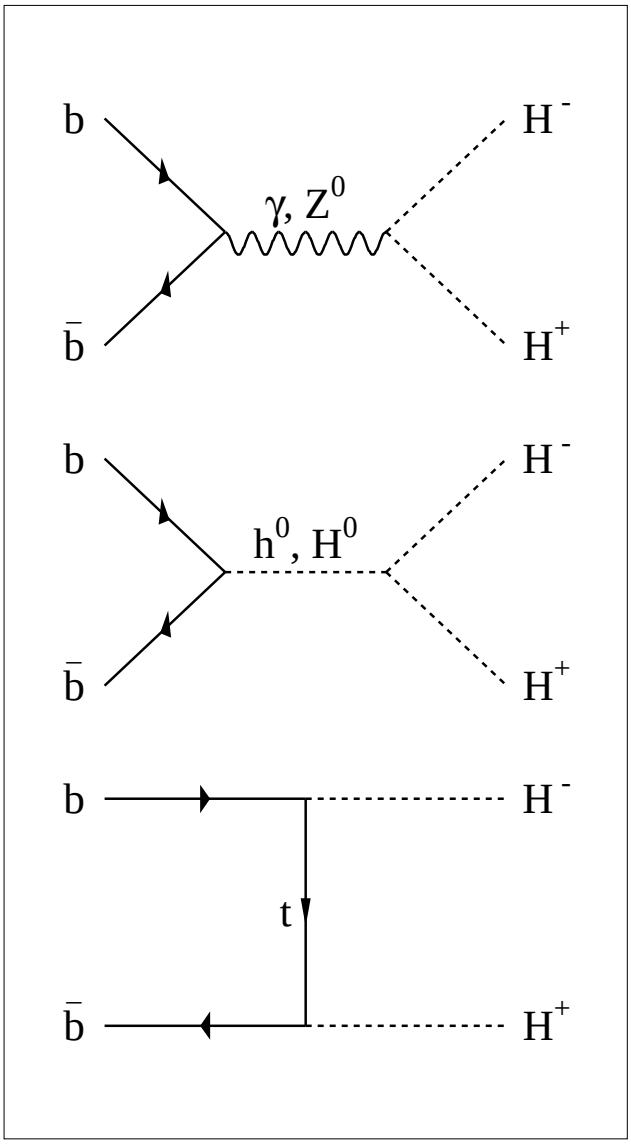

Figure 1: Tree-level Feynman diagrams for $b\bar{b} \to H^+H^-$ in the MSSM.

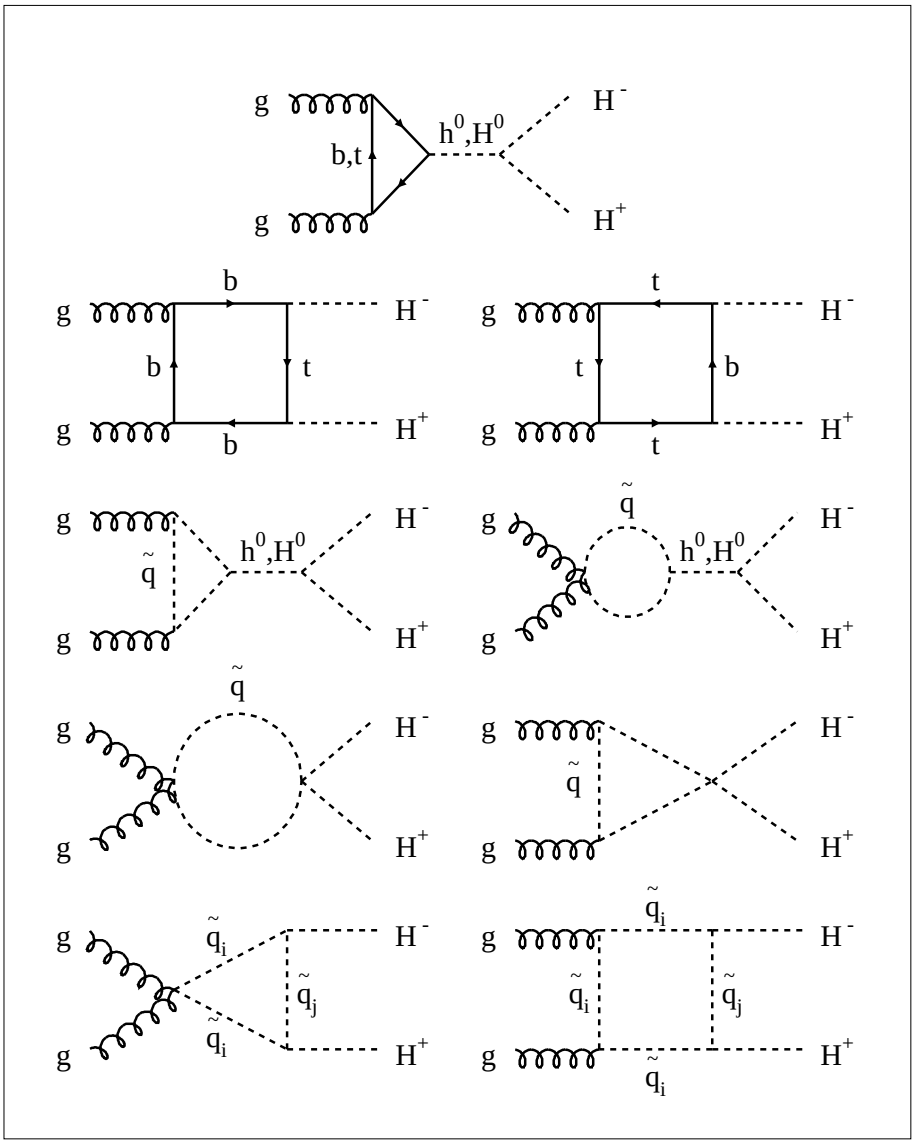

Figure 2: One-loop Feynman diagrams for $gg \to H^+H^-$ in the MSSM.

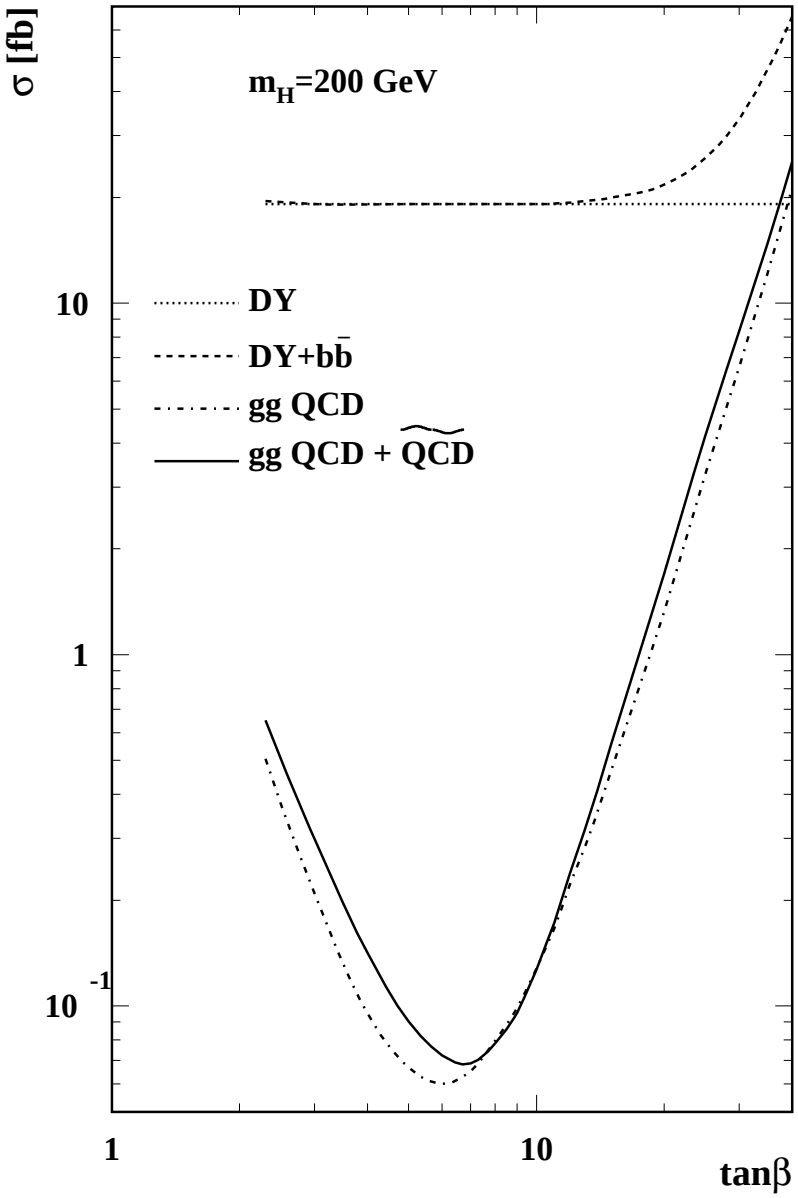

Figure 3: Total cross sections σ (in fb) of $pp \to H^+H^- + X$ via $q\bar{q}$ annihilation (dashed line) and gg fusion (solid line) at the LHC as functions of $\tan\beta$ for $m_H = 200$ GeV. For comparison, also the Drell-Yan contribution to $q\bar{q}$ annihilation (dotted line) and the quark loop contribution to gg fusion (dot-dashed line) are shown.

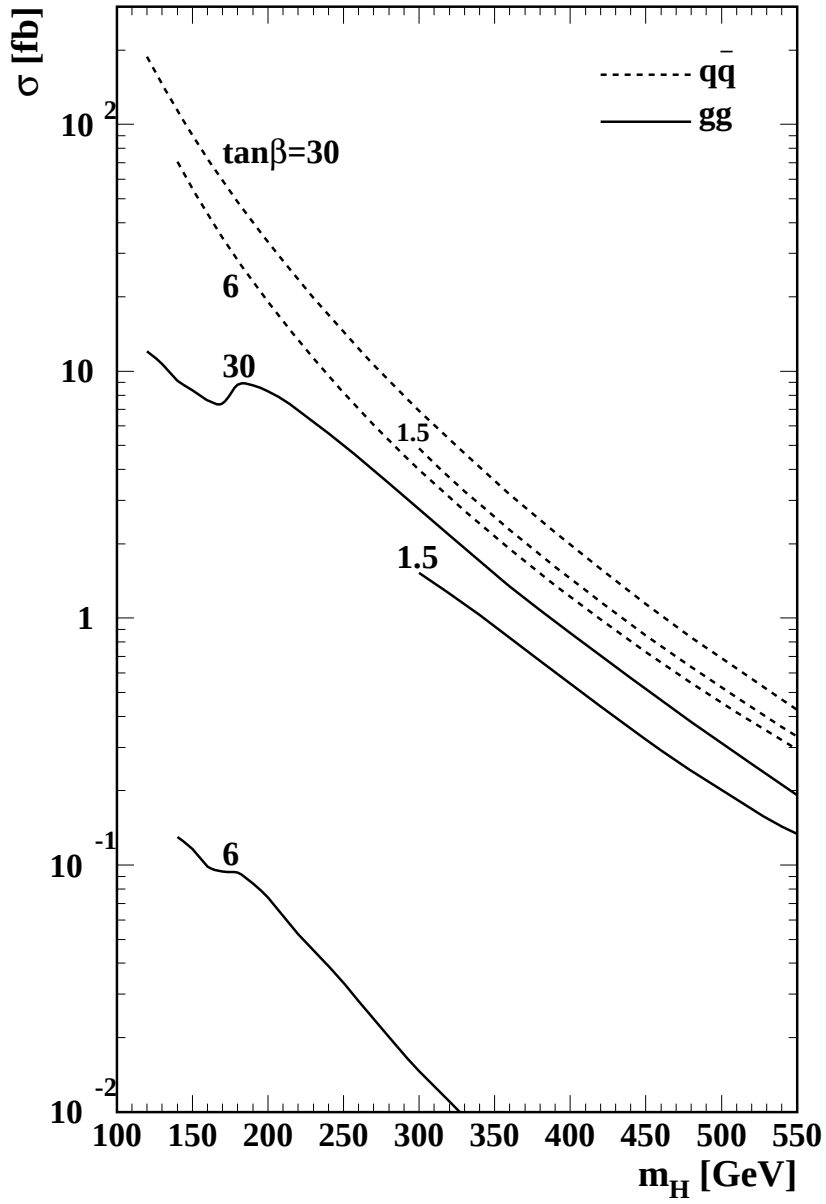

Figure 4: Total cross sections σ (in fb) of $pp \to H^+H^- + X$ via $q\bar{q}$ annihilation (dashed lines) and gg fusion (solid lines) at the LHC as functions of m_H for $\tan\beta = 1.5$, 6, and 30.